

# Modelling an actuated large deformation soft continuum robot surface undergoing external forces using a lumped-mass approach\*

Hossein Habibi, Chenghao Yang, Rongjie Kang, Ian D. Walker, Isuru S. Godage, Xin Dong & David T. Branson III

**Abstract** — Precise actuation of continuum surfaces in combination with continuum robotic arms that undergo large deformation is of high interest in soft robotics but of limited model-based study to date. This work develops this area towards enabling the robust design and control of large deformation continuum surfaces (LDCS) across multiple industrial applications in the healthcare, aerospace, manufacturing, and automotive domains. It introduces an actuation based dynamic model of LDCSs to accurately determine their deflection due to application of concentrated external forces while maintaining many physical characteristics and constraints on actuation elements and surface structure such as gravity, inertia, damping, elasticity, and interactive forces between actuators and LDCS. Using the lumped-mass methodology, a 3D integrated surface-arm model is developed, simulated and then validated experimentally where a pair of parallel arms are attached to the surface to actuate and deform it. The surface is then simultaneously subjected to a concentrated constant external force at its top center between the two arms. Comparing measured displacements between the experimental and modelling results over actuation time yielded the maximum error is less than 1% of the length of the surface's side at its final deflected profile despite the limited number of nodes (masses) used in the LDCS model while it is exposed to a significant external force.

## I. INTRODUCTION

Soft and compliant robotics is a rapidly emerging area within robotics. Research in the area is stimulating increasing interest in studying its more challenging aspects including development of kinematic and dynamic models and compliant control approaches for, and the design and manufacturing of, soft and compliant structures. There have been some significant developments in the field, particularly for continuum arms and manipulators as reported in the literature ([1], [2], [3], [4], [5]). These compliant robots are commonly employed in a wide range of applications in healthcare [6] and other areas such as inspection [7].

One potentially highly versatile structure in soft robotics of developing interest is that of large deformation continuum surfaces (LDCS) actuated by continuum arms. In this case a flexible surface is actuated into multiple curvature profiles by

integrated continuum arms as shown in Fig. 1. Such surfaces have the potential to be used for industrial purposes, for example as alternatives to conventional, reconfigurable moulding surfaces used in shaping relatively soft composite or alloy sheets. They can be also used as healthcare systems such as controllable exoskeletons [6].

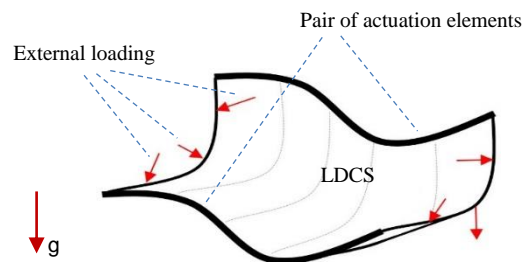


Figure 1. Representation of a large deformation continuum surface (LDCS) actuated by a parallel pair of integrated actuators while undergoing external forces

To date, the main loads analyzed for LDCSs in simulated environments are from the interactive forces applied by their actuation elements. However, actuated LDCSs are also subject to external and ambient forces in almost any projected application including healthcare, manufacturing, and food processing. The failure to account for these forces can significantly affect the performance of such surfaces in terms of controllability.

Examples of work in robotics focusing on external forces applied to mechanical flexible systems can be readily found in the literature ([8], [9], [10]). Typically, the first step to predict or control external forces in robotics is having a dynamic model that accurately simulates the effects of these forces applied to the flexible system. The focus of this paper is to develop a dynamic model for actuated LDCSs undergoing forces considered strong in comparison to their own weight and size characteristics. In future, such a model could be utilized to formulate control methods to enhance performance.

\* Research supported by UK Engineering and Physical Sciences Research Council (EPSRC).

H. Habibi was with the Faculty of Engineering, University of Nottingham, Nottingham, United Kingdom. He is now with the School of Science, Engineering & Design, Teesside University, Middlesbrough, TS1 3BX, UK (e-mails: [H.Habibi@tees.ac.uk](mailto:H.Habibi@tees.ac.uk); [Hossein.Habibi1@nottingham.ac.uk](mailto:Hossein.Habibi1@nottingham.ac.uk)).

C. Yang and R. Kang are with Key Laboratory of Mechanism Theory and Equipment Design of Ministry of Education School of Mechanical Engineering, Tianjin University, Tianjin, China (e-mails: [chenghao\\_yang@tju.edu.cn](mailto:chenghao_yang@tju.edu.cn), [rjkang@tju.edu.cn](mailto:rjkang@tju.edu.cn)).

I. D. Walker is with the Department of Electrical & Computer Engineering, Clemson University, Clemson, SC 29634-0915, US (email: [iwalker@clemson.edu](mailto:iwalker@clemson.edu)).

I. S. Godage is with the School of Computing, DePaul University, Chicago, IL 60604, email: [igodage@depaul.edu](mailto:igodage@depaul.edu).

X. Dong and D.T. Branson are with the Faculty of Engineering, University of Nottingham, Nottingham, United Kingdom (e-mails: [Xin.Dong@nottingham.ac.uk](mailto:Xin.Dong@nottingham.ac.uk), [David.Branson@nottingham.ac.uk](mailto:David.Branson@nottingham.ac.uk)).

In comparison to the fairly extensive studies on development of continuum arms and manipulators, there have been very limited studies to date carried out for LDCSs that investigate and simulate their deformation into a precise, desired profile. As a result, realizations of LDCSs have been mainly achieved through ‘trial and error’ based approaches that leads to increase in production cost and operation time while decreasing the resolution of their performance. One challenge in modelling these surfaces using classic plate and shell theories is that most of the existing techniques are only applicable to thin surfaces of small or negligible thickness (such as Kirchhoff–Love plate theory) without considering bending shear effects. Other theories that consider of thick plates (such as Mindlin–Reissner theory of plates) cannot be analytically employed for the large scale of deflection caused by robotic actuators. Hence, numerical solutions are sought to model actuation of LDCSs and determine their deformation with high resolution under a variety of conditions, e.g. when they are subjected to significant external forces.

In a study by Kano et al [11], a planar discretised model was developed for a sheet-like robot. The surface model underwent relatively large bending but some influential factors such as gravity, thickness and the moment of inertia effects along the planar coordinates were not included in the model. Another approach named as *phantom muscle method* is presented by Merino et al [12] which details a kinematic model for LDCSs by interpolating an infinite number of curves parallel to a single actuator attached to one edge of the surface when bent. This mathematical model is relatively computationally efficient, but does not present a high-resolution dynamic model as some important parameters such as material properties, elastic characteristics, external forces and gravitational effects have not been considered in its development.

In contrast, the model presented in this work to simulate actuation of LDCSs accounts for physical properties such as mass, material damping and elasticity, interactive forces between actuating arm and the surface, gravitational and external loading as well as the bending shear effects considered for thick plates. This work builds upon previous work [13] to apply a lumped-mass model for such actuated continuum surface robots by considering the feasibility and effect of applying external loading to these surfaces.

The paper is organized as follows. Section II describes the development of a lumped mass LDCS model actuated by a previously developed continuum arm model. In Section III, simulation results for the developed LDCS model actuated by two parallel continuum arm and subjected to an external force are presented. Section IV describes a test rig and experimental testing, while comparing empirical and modelling results to evaluate validity and dynamic performance of the developed model under external forces. Finally, the paper ends with a summary of the work, conclusions and further comments in Section V.

## II. MODELLING LDCS USING LUMPED MASS-SPRING-DAMPER ARRAYS

A lumped-mass approach has been utilized in this work to model LDCSs based on mass-spring-damper arrays. The

general modelling technique has been used previously in different studies particularly for its adaptability with large deflections [14], computational efficiency despite reliable accuracy ([15] and [16]), and its ability to represent an extensive range of robotic systems and structures whether they have obviously lumped characteristics, such as segmented manipulators ([16] and [17]), or they are more distributed systems, e.g. beams and surfaces ([18], [19] and [14]).

This paper presents a new development in a 3D, lumped-mass approach to model actuated two-layer LDCSs that can be deformed into curvatures resulting from a combination of loads applied by continuum arms, gravity and external forces. The general concept of the model is depicted in Figure 2. Despite the lumped-mass method being used for a wide range of applications, no research has been reported to date on development of a three-dimensional, multi-layer surface model that account for in-depth bending shear effects of thick flexible plates. Previous research has either modelled a single layer with negligible thickness or multi-layer, solid-like objects that cannot comply with the large deformations caused by continuum surface robots.

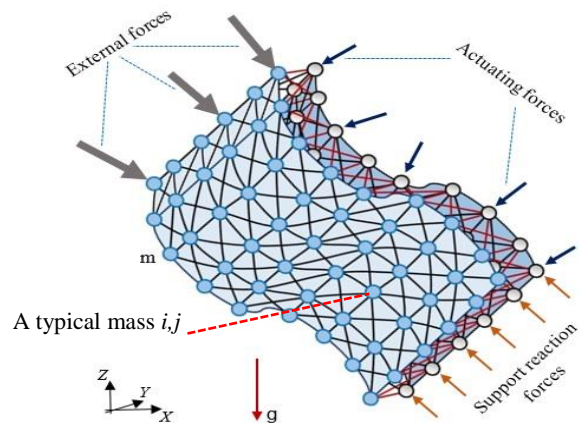


Figure 2. General concept of the developed 3D, lumped mass model composed of a 2-layer lattice of mass-spring-damper while subjected to different types of loading

The model is composed of masses considered as nodes in two joint lattices that are connected together through linear springs and dampers. Each mass is subjected to the linear momentum applied by gravity and the motion of neighbouring masses exerted through springs, while some also undergo direct external loads, boundary conditions such as clamped support reaction forces, or the interactive forces and moments applied directly by the actuators embedded in the surface.

As seen in Figure 2, each mass in the developed model is connected to 8 neighboring masses through 8 linear springs in the layer it is located in. The mass is also linked to 9 other masses positioned on the opposite layer. This means that a typical mass in one of the two layers is surrounded by 17 masses in total, among which 8 masses from the opposite layer are linked by diagonally-oriented springs which enables the model to take thickness bending shear effects into account. Although not noted elsewhere in this work, any spring depicted or mentioned is collocated with a linear

damper of damping coefficient  $c$  which are used to absorb vibrations due to movement and deformation of the surface.

In this work, the surface is assumed not to be constrained in any particular axis while the actuator model is confined to move in the XZ plane as shown in Fig. 3. Before actuation, the sides of LDCS model are flat and their main axes are straight. However the planes of the surface that are perpendicular to the neutral plane at rest do not remain perpendicular after deformation, as would be anticipated in the surface models and plate theories that account for in-depth shear effects [20]. The surface's material is considered isotropic and uniformly distributed across its rectangular, 2-layer geometry.

To characterize the dynamic behavior of the flexible LDCS, the equation of motion and consequently the displacement of a typical mass in the model indexed by ' $i,j$ ' (indicated in Figure 2) that moves in the direction  $q$  from its origin at time  $t_1$  to another point in the space at time  $t_2$  is yielded via combination and direct application of Newton's second law and Hooke's law as follows

$$\begin{aligned} u_q^{i,j} &= \int_{t_1}^{t_2} \left( \int_{t_1}^{t_2} \ddot{u}_q^{i,j} dt \right) dt \\ &= \frac{1}{m} \int_{t_1}^{t_2} \left( \int_{t_1}^{t_2} \sum F_q(t) dt \right) dt \\ &= \frac{1}{m} \int_{t_1}^{t_2} \left( \int_{t_1}^{t_2} \{k_q \delta U_q + c_q \frac{d}{dt} [\delta U_q] \right. \\ &\quad \left. + F_{(ext)q} - W\} dt \right) dt \end{aligned} \quad (1)$$

where  $q = x, y, z$  are Cartesian coordinates. Likewise,  $k_q$  and  $c_q$  are the stiffness of the spring and damping coefficient in direction  $q$  respectively. Note that the value of parameters  $k_q$  and  $c_q$  in (1) have been assumed constant and the same is true for all springs and dampers between any two masses in any direction throughout the LDCS model in this particular case which makes the surface uniform in terms of stiffness. So the variable  $\delta U_q$  is determined as the following

$$\begin{aligned} \delta U_q &= u_q^{i-1,j} + u_q^{i+1,j} + u_q^{i,j+1} + u_q^{i,j-1} + u_q^{i+1,j+1} + u_q^{i+1,j-1} \\ &+ u_q^{i-1,j+1} + u_q^{i-1,j-1} + u_q^{(i-1,j)_T} + u_q^{(i+1,j)_T} + u_q^{(i,j+1)_T} + u_q^{(i,j-1)_T} \\ &+ u_q^{(i+1,j+1)_T} + u_q^{(i+1,j-1)_T} + u_q^{(i-1,j-1)_T} + u_q^{(i,j)_T} \end{aligned} \quad (2)$$

In (2), the surrounding masses are indexed by  $i,j$  to identify positions and directions in the plane, where  $i$  stands for the x-direction and  $j$  for the y-direction. The mass indexed by  $i,j$  in (1) is on the bottom layer of the model. Hence the index  $T$  in (2) represents the masses located in the top layer of the model. As seen in (2), there are 17 terms included in  $\delta U_q$  which correlates to the 17 masses positioned in the two layers of the model that surround the typical mass  $i,j$ . Note that the number of surrounding masses and consequently the number of terms in (2) for the masses located on the edges and corners are reduced to 11 and 7 respectively. The number of equations to be solved is then equal to the total number of masses included in the model multiplied by 3 (the number of coordinates) which were solved for through a simulation implemented in the commercial software MATLAB R2016a.

The resultant of all forces acting on the typical mass  $i,j$  including those applied by the neighbouring masses through linear springs and dampers is represented by  $F_q(t)$  in (1). The two parameters  $F_{(ext)q}$  and  $W$  represent the external forces acting on the mass in the direction  $q$  and gravity applied in the direction  $-Z$  respectively. In our previous work on actuated LDCSs [13], the assumption  $F_{(ext)q}=0$  was considered in the model development. In this work the term  $F_{(ext)q}$  in (1) is explicitly included to account for external loading of the surface. We note that the term including  $c_q$  i.e. the damping force is actively effective in suppressing oscillations in the transient state before the flexible surface has settled into its final deformed shape. This term is then eliminated in steady-state conditions.

For the masses linked to actuators, the amount of displacement in the surface is initially dictated by the motion of the actuator attached at that point. The general concept of the arm model used here to actuate and deform the surface into desired curvatures has been previously developed and experimentally validated by Giri and Walker [21] wherein a section of a pneumatic continuum arm is modelled using lumped model elements and application of Lagrangian and virtual work principles. Then some minor changes and adjustments were made to the developed arm model in [21] to match it for integration with the developed LDCS model as seen in Figure 3. The main change is that, instead of input forces representing pneumatic muscles in the original model, input torques are applied to the links to rotate each link as  $\theta_i$  and consequently bend the whole arm.

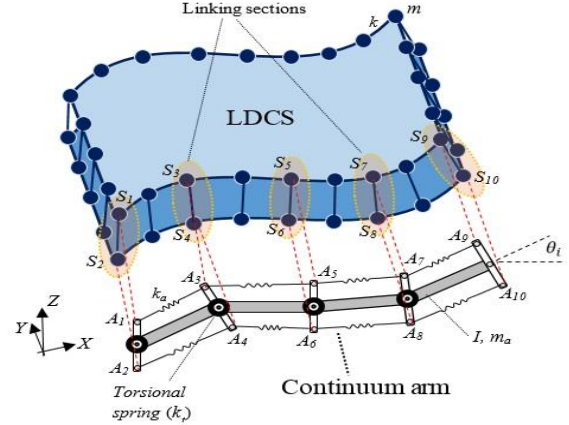


Figure 3. Schematic illustration of the LDCS model integrated with a continuum arm model linking together in five sections as indicated by the transparent ovals.

Note that for clarity and simplicity, only a few connecting links and their masses in the LDCS model have been depicted in Figure 3, far fewer than the actual number implemented in the model. An actual configuration between the links and masses is partially displayed in Figure 2.

As shown in Figure 3, the arm model adopted and adapted here consists of 4 main links of mass  $m_a$  and moment of inertia  $I$  which are joined together through torsional springs of stiffness coefficients  $k_t$ . Perpendicular to each main link, a massless link indicated by  $A_i A_{i+1}$  ( $i=1, 2, \dots$ ) in Figure 3, is rigidly connected which transfers the motion of the central backbone of the arm model to the LDCS model. The links  $A_i A_{i+1}$  in the arm model, which simulate the continuum

actuators used in the experiments described in section IV, are attached to the top and bottom borderlines of the LDCS model i.e. the mass-spring links  $S_i S_{i+1}$  ( $i=1, 2, \dots$ ), as shown in Figure 3, through springs stiffer than those used in the surface itself. So the length of each link  $A_i A_{i+1}$  are equal to the thickness of the surface or the free length of springs  $S_i S_{i+1}$ . The arm used in this study is assumed to move only in a plane, which for the current case shown in Figure 3 results in movement in the  $XZ$  plane, but further planar movement is possible through additional manipulation of the terms.

### III. SIMULATING THE INTEGRATED LDCS-ARM MODEL UNDER EXTERNAL LOADING AND GRAVITY

As mentioned previously, the main goal for the modeling of the actuated surface herein was to evaluate against external loading. For this reason the configuration shown schematically in Figure 4 was developed wherein an additional mass representing a concentrated, constant external force ( $F_0$ ) is applied to the top, centre of the surface at point  $P_1$  while the pair of arm models illustrated in Figure 3 are linked to two parallel edges of the LDCS model to simulate the embedded actuators. The surface in this configuration is clamped along the indicated edge to hold the surface up from the ground. Two points indicated as  $P_0$  and  $P_1$ , both located on the central, longitudinal axis of the surface, were specified to be measured for displacement due to actuation. Point  $P_0$  is located at the centre of the surface on both  $X$  and  $Y$  axes.

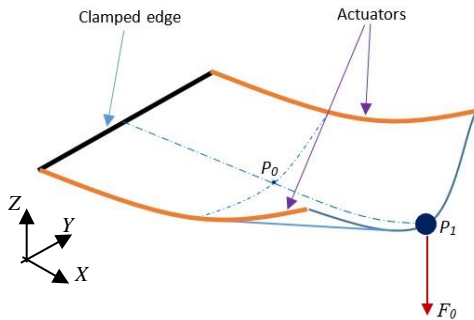


Figure 4. Schematic configuration of the test to simulate integrated LDCS-continuum arms model undergoing a significant statically-applied external force ( $F_0$ ).

For the tested model in this configuration, the surface was composed of two lattices of  $9 \times 9$  masses, or 162 masses in total across the surface. The value of each mass was chosen as  $m=9.87 \times 10^{-4}$  g to match the total mass of the fabricated surface (e.g.  $M=160$  g) for the experimental test described in the following section. The additional mass was the selected as  $m_0=40$  g (i.e. a quarter of the total mass of the surface) to determine the external load as  $F_0=0.39$  N. The spring stiffness used in the LDCS model demonstrated in the previous section was uniformly chosen as  $k_q=80$  N/m in all three directions  $q=x, y, z$  which conforms to the elasticity characteristics of the experimental surface model in the next section. Also a damping coefficient of  $c=5$  N.s/m was allotted to the model as the result of a compromise between the computational efficiency of the model and its oscillatory behaviour given other parameters. The two modelled and fabricated surfaces had identical geometrical dimensions as  $140 \times 140 \times 10$  mm.

The simulation results of this test are presented in Figure 5 wherein the 2-layer LDCS model has been bent up by two parallel continuum arms of identical physical properties embedded in the surface. The actuating arms are shown as black lines in the lateral side(s) of the LDCS model where they have displaced the surface by the curvature determined by the arm. In this test, actuating and gravity forces were applied simultaneously at the beginning. The surface is shown from two different views at its final static position after being actuated into a curvature of radius  $r=0.115$  m ( $k=8.69$  m<sup>-1</sup>) at the actuated edges. It can be seen that the top centre of the surface where the additional mass is attached sags down due to the concentrated external force applied to this point.

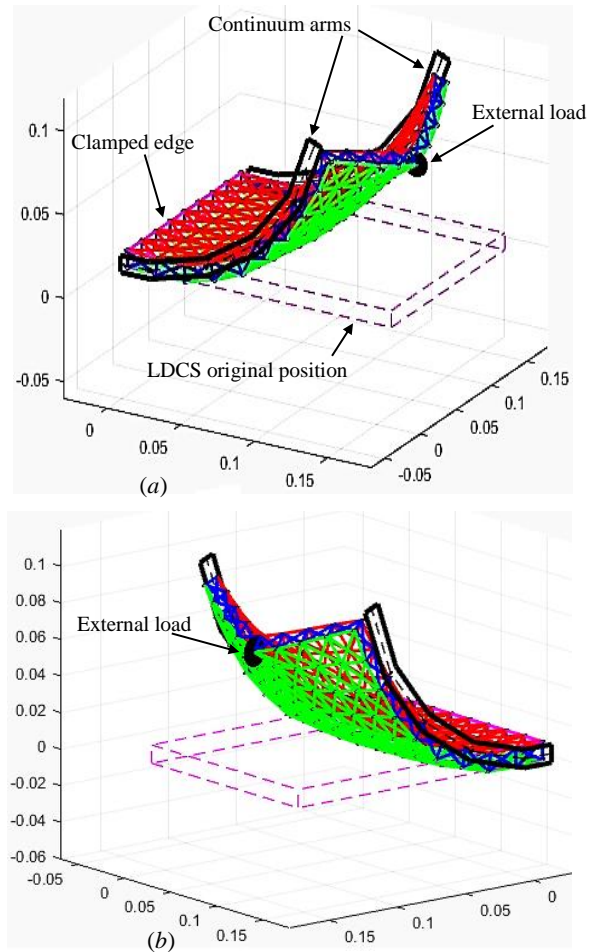


Figure 5. Simulation results from two different views (a, b) for the lumped mass LDCS model undergoing a concentrated external force displayed at its final static deformed shape after actuation by two continuum arms embedded in its two parallel edges.

### IV. EXPERIMENTAL TESTS AND COMPARISON WITH SIMULATION RESULTS

This section provides details on the testing procedure wherein experimental testing was conducted to validate simulation results for the developed actuated LDCS model.

#### A. Test rig setup

The experimental test was implemented through the test rig shown in Figure 6 which includes a support frame, sensor

system, data acquisition computer, and a pneumatic system to pressurise and operate the continuum actuators. The pneumatic arms, as illustrated in Figures 6 and 7, are located horizontally on two rigid plates of one-third of the surface's length as partial support for the integrated surface-arm before actuation. To apply the concentrated external force, an additional weight of mass  $m_0=40$  g was hooked to the top centre of the surface as indicated in Figures 6 and 7.

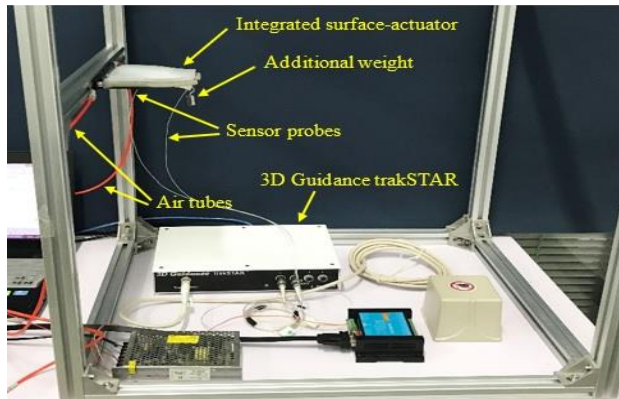


Figure 6. Experimental test rig setup.

The sensor used is a 3D Guidance trakSTAR (Ascension Corp., USA, 0.1 mm accuracy). It also has three sensor probes that can be attached to the surface at any desired position for further measuring displacement. Both the flexible surface and continuum arms were fabricated from silicon rubber poured and formed into designed moulds. An inextensible layer was then used for the arm to be adapted and integrated with the surface. Further details on manufacturing, operation, and controlling of this arm can be found in [22]. In this experiment, an air pressure of 1.4 bar was applied to bend the surface carrying the additional mass into a curvature of radius  $r=0.115$  m as resulted in the simulation. To approximate Young's modulus ( $E$ ) of the manufactured surface, a simple tensile test was carried out that yielded it as  $E=75.35$  kPa. Also, the Poisson's ratio of the surface, made from the incompressible material, silicon rubber, was chosen as 0.5 [23].

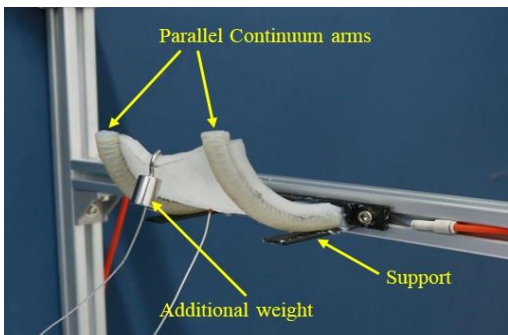


Figure 7. Image of the experimental test of the actuated flexible surface undergoing an additional weight positioned between two embedded continuum arms.

### B. Experimental results and comparisons

Once the two arms were embedded on the surface as a pair of parallel actuators, they were operated by gradually increasing air pressure to bend the surface upwards while undergoing an external load into the desired curvature as resulted in the simulation test. Figure 7 shows the final

deformation of the integrated actuator-surface after the transient operation of actuation ended. During the test, two sensors were attached to the points  $P_0$  and  $P_1$  (as indicated in Figure 4) to measure and record their displacement over the entire actuation period. This was done to evaluate the dynamic performance of the developed LDCS model when it was exposed to both gravity and significant concentrated external forces simultaneously. Figure 8(a, b) show the displacement of point  $P_0$  and  $P_1$  versus time in the three directions x, y and z for both the modelling and experimental tests.

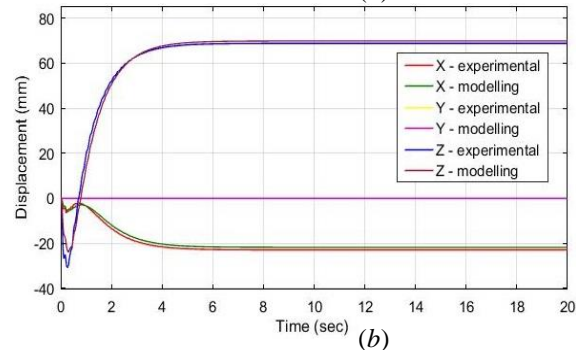
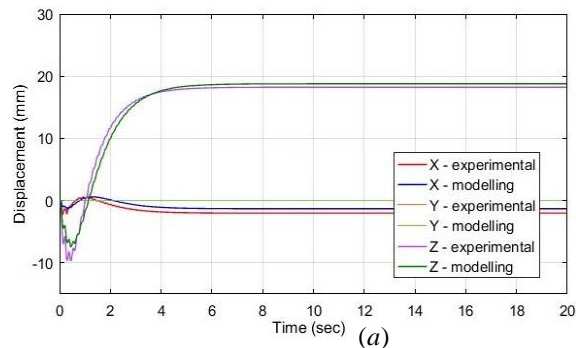


Figure 8. Comparing the dynamic behaviour of the modelled LDCS and the empirical surface through recording the displacement of the points a)  $P_0$ , and b)  $P_1$  as indicated in Figure 4 over time in the three direction X, Y, and Z.

As seen, the points undergo tiny fluctuations in displacement in the transient initial period, due to the sudden addition of the mass. Differences in this transient region are small and likely due to material property differences in the model. After the transient dies out the two results converge and settle very close together in the X and Z directions, indicating a reliable static performance of the developed model. The results in direction Y remain zero as expected due to symmetry in geometry, loading, and boundary conditions applied by the two parallel arms positioned equally apart on its two sides. For further clarity, the steady state displacements of these two points in the three directions for both modelling and experimental tests along with their absolute errors are presented in Table I.

As seen in Table I, the measured points  $P_1$  i.e. the point to which the additional mass is attached, as expected, undergoes the largest displacement of the surface in direction Z with an absolute error of 1.2 mm which is less than 1% of the length of the surface's side at its final reshaped profile.

### V. CONCLUDING REMARKS

In this study, a 3D, lumped-mass model consisting of two interconnected mass-spring-damper lattices subjected to

external forces while actuated by integrated continuum robotic arms was developed and validated experimentally. The configuration of the surface model enabled deformation resulting from a combination of loads applied by the actuation arms, gravity and external forces while accounting for in-depth bending shear effects of thick flexible plates. The model successfully demonstrated the dynamical performance of actuated surfaces undergoing large deformation while they experienced concentrated external loading that significantly affected their dynamics. The conformity between modelling and experimental results, whether dynamically over the transient actuation time or statically after the end of motion, was considerable with a maximum error less than 1% of the length of the surface's side at the final deflected position. This development is of high interest in the field of soft and continuum robotics, particularly where undesirable external forces are of major concern. Important potential applications of this work include the manipulation of parts in manufacturing environments, soft/flexible exoskeleton systems in healthcare, and deformable surface control in the aerospace, automotive, energy and food processing industries.

TABLE I  
Comparison of the final displacement results between the LDGS model and the experimental surface (Figure 5 and Figure 7) measured at 2 central points of the surface.

Measured Points		Displacement (mm)		
		Modelling	Experimental	Error
P <sub>0</sub>	$u_x$	-1.3	-2.0	0.7
	$u_y$	0	0	0
	$u_z$	18.8	18.2	0.6
P <sub>1</sub>	$u_x$	-21.8	-22.9	1.1
	$u_y$	0	0	0
	$u_z$	69.9	68.7	1.2

#### ACKNOWLEDGMENT

This work is funded and supported by the Engineering and Physical Sciences Research Council (EPSRC) under grant number: EP/N022505/1, and the Natural Science Foundation of China (NSFC) under grant number: 51611130202.

#### REFERENCES

[1] I. D. Walker, "Continuous Backbone "Continuum" Robot Manipulators," *ISRN Robotics*, vol. 2013, pp. 1-19, 2013.

[2] I.S. Godage, G.A. Medrano-Cerda, D. Branson, E. Guglielmino and D.G. Caldwell, "Dynamics for Variable Length Multisection Continuum Arms," *The International Journal of Robotics Research*, vol. 35, no. 6, pp. 695-772, 2016.

[3] B. L. Conrad, J. Jung and R. S. Penning, "Interleaved continuum-rigid manipulation: An augmented approach for robotic minimally-invasive flexible catheter-based procedures," *IEEE International Conference on Robotics and Automation*, pp. 718-724, 2013.

[4] E. Tatlicioglu, I. D. Walker and D. M. Dawson, "Dynamic Modelling for Planar Extensible Continuum Robot Manipulators," in *IEEE International Conference on Robotics and Automation*, pp. 1357-1362, Roma, 2007.

[5] J.L.C. Santiago, I.D. Walker, and I.S. Godage, "Continuum robots for space applications based on layer-jamming scales with stiffening capability," in *IEEE Aerospace Conference*, 2015: 1-13.

[6] J. Burgner-Kahrs, D. C. Rucker and H. Choset, "Continuum Robots for Medical Applications: A Survey," *IEEE Transactions on Robotics*, vol. 31, no. 6, pp. 1261-1280, 2015.

[7] X. Dong, D. Axinte, D. Palmer, S. Cobos, M. Raffles, A. Rabani, and J. Kell, "Development of a Slender Robotic System for On-Wing Inspection/Repair of Gas Turbine Engines," *Robotics and Computer-Integrated Manufacturing*, vol. 44, pp. 218-229, April 2017.

[8] W.J. O'Connor, and H. Habibi, "Wave-based control of under-actuated flexible structures with strong external disturbing forces," *International Journal of Control*, vol. 88, no. 9, p. 1818-1829, 2015.

[9] J. Qin, F. Léonard and G. Abba, "Experimental external force estimation using a non-linear observer for 6 axes flexible-joint industrial manipulators," in *IEEE Control Conference (ASCC), 2013 9th Asian*, Istanbul, Turkey, 2013.

[10] Y. Noh, E.L. Secco, S. Sareh, H. Wurdemann, A. Faragasso, J. Back, H. Liu, E. Sklar and K. Althoefer, "A continuum body force sensor designed for flexible surgical robotics devices," in *Conf Proc IEEE Eng Med Biol Soc*, 2014:3711-4. doi: 10.1109/EMBC, 2014.

[11] T. Kano, Y. Watanabe, and A. Ishiguro, "Sheetbot, Two-dimensional sheet-like robot as a tool for constructing universal decentralized control systems," in *IEEE International Conference on Robotics and Automation (ICRA)*, 2012: 3733-3738.

[12] J. Merino, A. L. Threatt, I. D. Walker and K. E. Green, "Forward Kinematic Model for Continuum Robotic Surfaces," in *IEEE/RSJ International Conference on Intelligent Robots and Systems (IROS)*, pp. 3453-3460, Vilamoura, Algarve, Portugal, 2012.

[13] H. Habibi, C. Yang, R. Kang, I.D. Walker, I.S. Godage & D.T. Branson III, Developing a 3-D, lumped-mass model to present behaviour of large deformation surface based continuum robots, Book chapter in *Springer IUTAM Bookseries*, (accepted for publication following revisions).

[14] T. Liu, A.W. Bargteil, J.F. O'Brien, and L. Kavan, "Fast simulation of mass-spring systems," *ACM Transactions on Graphics*, vol. 32, no. 6, pp. 1-7, 2013.

[15] J. Mesit, R. Guha, and S. Chaudhry, "3D Soft Body Simulation Using Mass-spring System with Internal Pressure Force and Simplified Implicit Integration," *Journal of computers*, vol. 2, no. 8, pp. 34-43, October 2007.

[16] H. Habibi and W. O'Connor, "Wave-based control of planar motion of beam-like mass-spring arrays," *Wave Motion*, vol. 72, p. 317-330, 2017.

[17] M. Dehghani and S.A. Moosavian, "Dynamics Modeling of a Continuum Robotic Arm with a Contact Point in Planar Grasp," *Journal of Robotics*, vol. 2014, no. Article ID 308283, p. 13 pages, 2014.

[18] J. Anthonis, and H. Ramon, "Comparison between the discrete and finite element methods for modelling an agricultural spray boom - Part 1: Theoretical derivation," *Journal of Sound and Vibration*, vol. 266, p. 515-534, 2003.

[19] M. Kino, T. Murakami, and K. Ohnishi, "A vibration suppression and disturbance rejection strategy of flexible manipulator by multiple acceleration feedback," in *Proceedings of Movic '98, Vol. 2*, pp. 781-786, Zurich, 1998.

[20] J.N. Reddy, Theory and analysis of elastic plates and shells, CRC Press, Taylor and Francis, 2007.

[21] N. Giri, I.D. Walker, "Three Module Lumped Element Model of a Continuum Arm Section," in *2011 IEEE/RSJ International Conference on Intelligent Robots and Systems*, San Francisco, CA, USA, 2011.

[22] P. Polygerinos, Z. Wang, J.T.B. Overvelde, K.C. Galloway, R.J. Wood, K. Bertoldi, and C.J. Walsh, "Modeling of soft fiber-reinforced bending actuators," *IEEE Transactions on Robotics*, vol. 31, no. 3, pp. 778-789, 2015.

[23] G.N. Greaves, A.L. Greer, R.S. Lakes and T.Rouxel, "Poisson's ratio and modern materials," *Nature Materials*, vol. 10, pp. 823-837, 2011.